International Journal of Solids and Structures 48 (2011) 2275–2287

Contents lists available at ScienceDirect

International Journal of Solids and Structures

journal homepage: www.elsevier.com/locate/ijsolstr

A constitutive model for the mechanical response of the folding of creased paperboard

A. Giampieri [a], U. Perego [a,*], R. Borsari [b]

[a] Department of Structural Engineering, Politecnico di Milano, Piazza L. da Vinci, 32, 20133 Milan, Italy
[b] Tetra Pak Packaging Solutions, via Delfini 1, 41100 Modena, Italy

ARTICLE INFO

Article history:
Received 15 February 2011
Received in revised form 28 March 2011
Available online 20 April 2011

Keywords:
Paperboard
Crease
Shells
Interface finite element

ABSTRACT

Paperboard is a widely used material in industrial processes, in particular for packaging purposes. Packages are obtained through a forming process, in which a flat laminated sheet is converted into the final 3-D solid. In the package forming process, it is common practice to score the paperboard laminate with crease lines, in order to obtain folds with sharp edges and to minimize the initiation and propagation of flaws during the subsequent folding procedures. In this work, a constitutive model for the mechanical response of crease lines is proposed and validated on the basis of experimental tests available in the literature. The model has been implemented in an interface finite element to be placed between adjacent shell elements and is intended for large-scale computations of package forming processes. For this reason, the material model has been developed at the macroscopic scale in terms of generalized variables, aiming at computational effectiveness.

1. Introduction

Packaging is a key factor for the production and distribution of consumer goods and it is itself a fast growing industry. Reliable and economical packaging is required for storage, transportation and distribution, until the product is delivered to its final destination and the package is opened. Increasing consciousness of environmental issues and more advanced legislations together with expanding competition in this fast growing market are also driving the industry towards lighter, more economical, reliable and recyclable solutions, which require substantial investments in the development of new technological solutions.

Paperboard is one of the most widely used materials in the packaging industry, since it can be easily converted from a flat configuration into a box shaped solid. Carton boxes are light and at the same time can be very stiff and sustain significant loads. Paperboard packaging can be achieved in several ways, e.g. by erecting a 'skillet' (a flattened prefolded element of carton board) into a box shaped container, or by forming a box from a cylindrical sleeve filled with liquid, using mechanical clamps. In all cases, the final shape is achieved by folding the paperboard flat blank around predetermined lines. The final package performance depends heavily on the folding quality which has to produce well defined edges and corners, without damaging the container's external surface.

To facilitate paperboard folding around the prescribed lines, the paperboard blank is 'creased' before being converted into its final shape, i.e. the folding lines are scored onto the paperboard by pressing it into a grooved female die by a male die with a rule (Fig. 1a). The creasing produces a local, shear induced delamination into the paperboard structure which reduces its bending stiffness and promotes the folding around the design lines. After being creased, the paperboard presents a residual indent where the material is delaminated. The delamination extent depends on the creasing severity (i.e. the indentation depth h) and on the creasing tool geometry (width W of the groove in the female die and width b of the rule of the male die).

In the present work, creasing of non-corrugated paperboard is considered. For recent studies on creasing and folding of corrugated paperboard, see e.g. Isaksson and Hagglund (2005), Harrysson and Ristinmaa (2008) and Thakkar et al. (2008).

Packaging paperboard is a layered material with typically 3 or more plies. Each ply consists of a network of fibers, entangled or chemically bonded together. The outer plies are usually stiffer (chemical pulp layers), while the inner plies (mechanical pulp layers) are softer. The forming process of the plies produces an orientation of the fibers in the lamination direction (machine direction, MD). Typically, the in-plane mechanical properties of the plies are such that stiffness and strength in cross-direction (CD) are a factor of two weaker than in MD. Individual plies are glued together, so that interfaces exist between plies. Stiffness and strength of the thicker middle layer in the out-of-plane direction are provided by weak bonds mainly due to fiber entanglement. Even though adhesion between plies can be improved using chemical treatments, stiffness and strength in the thickness direction (ZD) can be two orders of magnitude lower than in MD. The anisotropic

* Corresponding author. Tel.: +39 02 2399 4214; fax: +39 02 2399 4220.
E-mail address: umberto.perego@polimi.it (U. Perego).

0020-7683/$ - see front matter © 2011 Elsevier Ltd. All rights reserved.
doi:10.1016/j.ijsolstr.2011.04.002

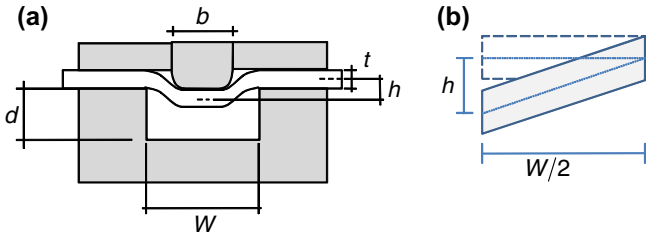

Fig. 1. (a) Schematic description of creasing tool. (b) Definition of initial shearing strain parameter γ.

paperboard behavior reflects on the crease behavior which depends on the crease line orientation with respect to the material orientation, especially for shallow creasing depth.

Accurate modeling of the crease behavior is a key ingredient for the design and possible numerical simulation of the package forming process. Besides the abundant literature on constitutive modeling of in-plane and through the thickness behavior of paper (see e.g. Sawyer et al., 1998; Xia, 2002; Xia et al., 2002; Stenberg et al., 2001; Castro and Ostoja-Starzewski, 2003; Makela and Östlund, 2003), there are in the literature a number of contributions specifically concerned with creasing and folding of paperboard. Carlsson et al. (1983) used a simple parallel beam model to account for stiffness loss in the creased region due to delamination and subsequent buckling of the compressed layers. Cavlin et al. (1997) proposed a creasability testing methodology based on the use of an inclined rule allowing to span different penetration depths in a continuous way in a single test. Nygårds et al. (2005, 2009) used a user defined subroutine, implemented in the finite element code Abaqus, to simulate the damage produced by the paperboard creasing and subsequent folding. The material model was inspired to the work of Xia et al. (2002) for the in-plane material behavior, with the addition of interface elements to account for delamination between layers. The numerical simulations were validated against experimental creasing tests showing good agreement. Beex and Peerlings (2009) proposed a contribution in the same line, whereby the results of a combined continuum-delamination numerical model constructed in the MSC.Marc finite element code are compared to the experimental creasing and folding results obtained on a relatively thick paperboard. Recently, Nagasawa et al. (2003) carried out an experimental campaign on thin coated paperboard aimed at assessing the effect of crease penetration and geometry on the subsequent folding behavior of the creased paper. In Nagasawa et al. (2008) the study was extended to aluminum coated and white-coated paperboard.

In the present paper, a material model, implemented in an interface finite element for the simulation of the crease presence in a curved shell structure, is presented. The interface element is designed to be placed between adjacent 4 node shell finite elements of the Mindlin–Reissner type and is formulated in terms of generalized internal forces (moments and forces per unit length) and strains (displacement jumps at the shell middle surface and relative rotations), allowing for large displacement and rotation jumps. The element is intended to be used in full-scale simulations of package forming processes and for the optimization of creasing patterns in paperboard or other thin membranes. The main feature of the constitutive model is therefore to be computationally inexpensive and to be based on a limited number of parameters. In this paper, the focus is on the formulation of the material model for the description of the membrane-bending behavior of a crease line, assuming that the parameters of the preceding creasing process are known, while a detailed description of the interface element kinematics can be found in Giampieri and Perego (2011). The material model accounts in a phenomenological way for the permanent elastoplastic deformation of paper and for both the initial and progressive damage due to paperboard creasing and subsequent folding. Particular attention has been devoted to the definition of the dependency of material parameters on the crease penetration depth. The model has been calibrated on the experimental results provided by Nagasawa et al. (2003) showing good agreement in the simulation of the folding tests.

2. Physical evidences of crease behavior during folding

Below, a brief account of the main features of the crease behavior during creasing and subsequent folding is reported, mainly based on the results of the experimental tests described in Nagasawa et al. (2003), Nygårds et al. (2009), Beex and Peerlings (2009).

Paperboard creasing is intended to facilitate folding along predefined lines during the paperboard transformation process from a flat blank into a 3D package. A creasing sequence is sketchily illustrated in Fig. 2. The paperboard blank is pushed by a male die with a rule into a groove of the female die. The rule can have sharp or rounded corners or, in certain cases, a rubber fixture. The rule and groove geometrical data (width, depth, relative clearance, geometry of the indenter) are important parameters which affect the final behavior of the creased material.

Paper is a layered material. The creasing produces a permanent delamination damage, promoted by interlaminar shear, in addition to in-plane and compressive out-of-plane plastic deformation of the plies, whose extent depends on the crease severity. For higher creasing levels, damage diffuses inside the individual layers starting from the softer mechanical pulp layers in the core of the laminate. These defects will represent initiation sites for propagation of delamination inside the middle layers during the subsequent folding of the crease (Beex and Peerlings, 2009).

When the rule is removed, the paperboard exhibits a residual indent which represents an initial planarity defect for the subsequent folding process. During folding, the delaminated layers on

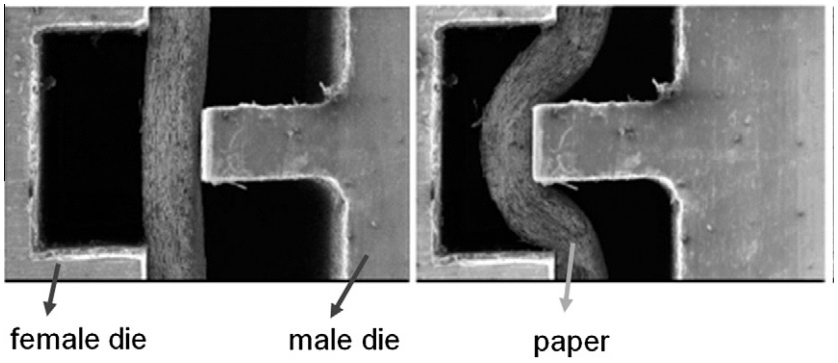

Fig. 2. Creasing sequence.

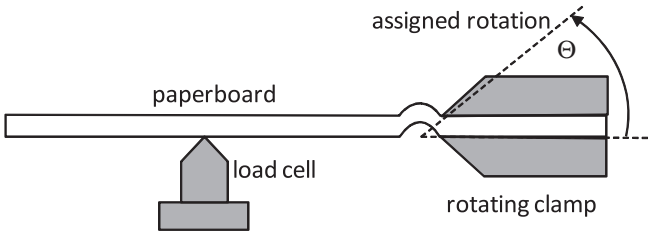

Fig. 3. Schematic description of bending test rig used in Nagasawa et al. (2003).

the compressed side are subjected to a compressive force and undergo large transverse deflections, promoted by the initial defect, under combined bending and compression. The bending and axial behavior of the delaminated layer is a consequence of the creasing operation: the width of the groove and the penetration depth affect not only the length and thickness of the delaminated layers, but also their initial deviation from planarity due to the plastic indent.

Nagasawa et al. (2003) carried out an extensive experimental investigation on paperboard creasing, trying to assess the mechanical effects of the creasing parameters. As a first step, to synthesize the characteristics of the creasing process, they defined the "nominal initial shearing strain" γ (Fig. 1b)

$$\gamma = \frac{2h}{W} \tag{1}$$

where h denotes the rule penetration depth and W is the groove width. γ is a nondimensional parameter, related to the initial shearing deformation imposed to the paperboard, as shown in Fig. 1b, which increases with the severity of the creasing process.

Using a carbon-steel rule of thickness $b = 0.72$ mm, tip radius $r = 0.36$ mm and a female die, with a groove of width $W = 1.5$ mm and depth 1.0 mm, they creased three types of paperboard of the same nominal grammage of 350 g/m^2 but of slightly different thickness and mechanical properties, both in transverse and parallel direction to MD.

After the creasing, the bending moment M_c versus rotation ϑ_c response of the creased specimen was measured using a testing rig of the type sketchily shown in Fig. 3, whereby one side of the specimen is secured by rotating clamps while the other one is contrasted by a load cell measuring the reaction force. The specimen is placed in the clamps in such a way that the crease line is aligned with the rotation axis of the clamps. Three specimens were tested for each value of initial strain γ, imposing rotations from 0° to 90°.

A sectional view of the deformation at 90° for different values of γ is shown in Fig. 4 for a transversally creased paperboard (i.e. the crease line is parallel to CD), with thickness $t = 0.46$ mm, surface density $\rho = 368$ g/m^2, tensile strength in MD $\sigma_0 = 45.8$ MPa. The M_c–ϑ_c response for varying γ is plotted in Fig. 5.

From the images of Fig. 4, it can be seen that: (i) for $\gamma = 0$ (non-creased specimen) the corner is not well defined and there is visible damage in the outer layer of the paperboard; very little delamination can be observed between the inner layers; (ii) for $\gamma = 0.61 \div 0.88$ the creasing appears to be optimal: the corner region is regular and well defined; there is no visible damage on the outer layer; the delamination inside the inner ply is contained within the crease region; the bulging profile is symmetric with respect to the crease axis; (iii) for higher values of γ, the crease width increases and the corners loose their definition with loss of symmetry: delamination extends outside the crease region, giving place to longer and longer delaminated layers.

The M_c–ϑ_c plot of Fig. 5 refers to bending of the same paperboard, transversely creased with different values of γ. From the plot one can qualitatively observe that: (i) for all values of γ, beyond a certain rotation, the creased paperboard exhibits a ductile bending behavior with an almost flat plateau up to a rotation of 90°; (ii) there exists a transition value $\gamma \approx 0.6$ for which the qualitative response changes; (iii) for $\gamma < 0.6$ (shallow crease), after an initially linear path, followed by a nonlinear hardening branch, the M_c–ϑ_c curve reaches a peak followed by a softening branch; the progression of delamination promoted by buckling of the compressed layers leads to an abrupt release of elastic energy with a sharp reduction of bending strength (Chai et al., 1981; Carlsson et al., 1983), followed by an almost perfectly plastic plateau; (iv) for growing values of $\gamma < 0.6$, the peak value M_c^{max} decreases and it is reached for decreasing values of the rotation angle ϑ_c; (v) for $\gamma \geqslant 0.6$ (deep creasing), damage progresses in a stable manner during folding, with a gradual energy release, and there is no visible peak, meaning that the damage process stops in correspondence to the activation of a plastic dissipation mechanism. This can be interpreted as being due to the fact that the initial damage produced by the deep creasing was already close to its maximum attainable value.

3. Crease interface kinematics and balance equation

The geometry of a shell body of thickness t in the original and deformed configurations can be described by the mappings

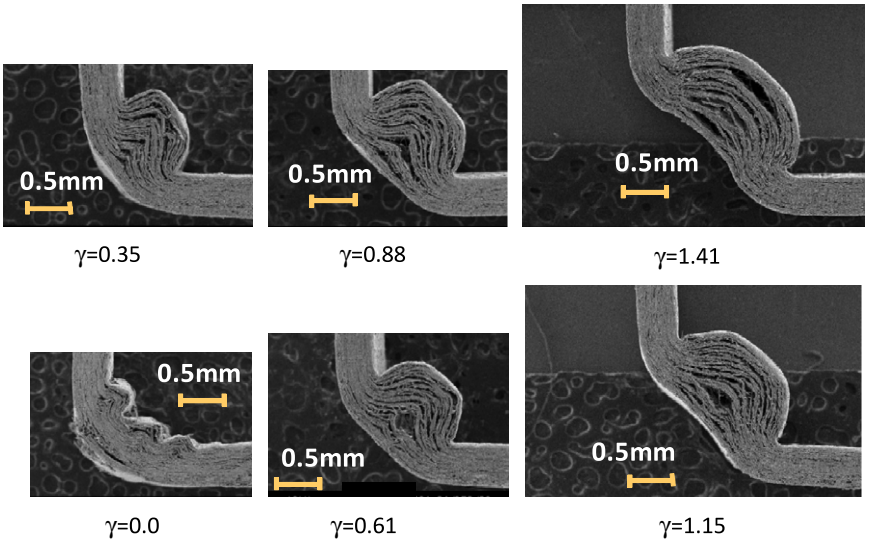

Fig. 4. 90° bending test on creased specimen (courtesy of Nagasawa et al. (2003)).

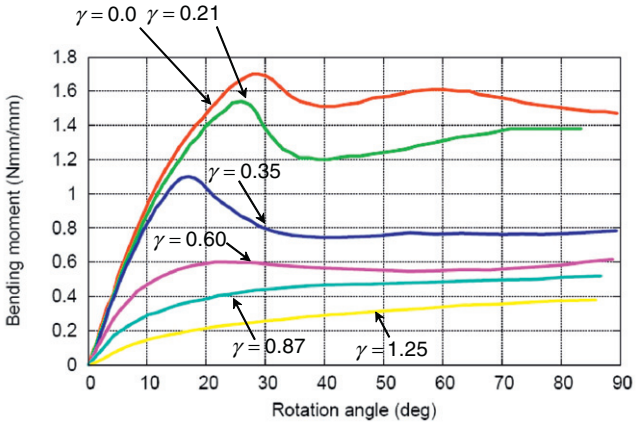

Fig. 5. M_c–ϑ_c response from bending tests for varying γ (Nagasawa et al., 2003).

$$\begin{aligned}\mathbf{X} &= \boldsymbol{\Phi}(\xi^1,\xi^2,\xi^3) = \overline{\boldsymbol{\Phi}}(\xi^1,\xi^2) + \xi^3\mathbf{T}(\xi^1,\xi^2)\\ \mathbf{x} &= \boldsymbol{\varphi}(\xi^1,\xi^2,\xi^3) = \bar{\boldsymbol{\varphi}}(\xi^1,\xi^2) + \xi^3\mathbf{t}(\xi^1,\xi^2) \quad -\frac{t}{2}\leqslant\xi^3\leqslant\frac{t}{2}\end{aligned} \tag{2}$$

where $\mathbf{X}$ in Eq. $(2)_a$ is the position vector of a material point in the shell body in the initial configuration, identified by the convective system of coordinates ξ^1,ξ^2,ξ^3; $\overline{\mathbf{X}} = \overline{\boldsymbol{\Phi}}(\xi^1,\xi^2)$ is the position vector of points belonging to the shell middle surface $\mathcal{M}$ ($\xi^3 = 0$), with boundary $\partial\mathcal{M}$, and the unit vector $\mathbf{T}(\xi^1,\xi^2)$ denotes the inextensible director field. Eq. $(2)_b$ describes the displaced configuration, with obvious meaning of symbols. According to the Mindlin–Reissner assumption, $\mathbf{T}$ is not forced to remain normal to the middle surface during the deformation.

The displacement $\mathbf{u}$ at a point $\mathbf{X}(\xi^1,\xi^2,\xi^3)$ follows from this kinematic description as

$$\begin{aligned}\mathbf{u}(\xi^1,\xi^2,\xi^3) &= \mathbf{x}(\xi^1,\xi^2,\xi^3) - \mathbf{X}(\xi^1,\xi^2,\xi^3)\\ &= \bar{\mathbf{u}}(\xi^1,\xi^2) + \xi^3\left[\mathbf{t}(\xi^1,\xi^2) - \mathbf{T}(\xi^1,\xi^2)\right]\end{aligned} \tag{3}$$

In the initial configuration, the crease region is described as a zero-thickness surface defined by its intersection Γ_c with the shell middle surface and the corresponding director field. Hence, points belonging to the interface are defined by the mapping

$$\mathbf{X}_c = \overline{\boldsymbol{\Phi}}_c(\xi^1(\zeta),\xi^2(\zeta)) + \xi^3\mathbf{T}_c(\xi^1(\zeta),\xi^2(\zeta)) \tag{4}$$

where $\overline{\boldsymbol{\Phi}}_c(\zeta)$ is the parametric representation of Γ_c on the middle surface and ζ is a scalar parameter.

In the deformed configuration, it is convenient to define the interface reference line as the average curve $\widetilde{\Gamma}_c$ between the two sides $\Gamma_c^+\times\left[-\frac{t}{2},\frac{t}{2}\right]$ and $\Gamma_c^-\times\left[-\frac{t}{2},\frac{t}{2}\right]$ of the interface, where the two curves, Γ_c^+ and Γ_c^- have the same parametric representation in terms of the convective coordinate ζ. (see Fig. 6). The deformed interface reference surface $\widetilde{\Gamma}_c\times\left[-\frac{t}{2},\frac{t}{2}\right]$ is then defined as the locus of points of coordinates

$$\tilde{\mathbf{x}} = \tilde{\bar{\boldsymbol{\varphi}}}(\xi^1(\zeta),\xi^2(\zeta)) + \xi^3\tilde{\mathbf{t}}(\xi^1(\zeta),\xi^2(\zeta)) \quad -\frac{t}{2}\leqslant\xi^3\leqslant\frac{t}{2} \tag{5}$$

where

$$\tilde{\bar{\boldsymbol{\varphi}}} = \frac{1}{2}(\bar{\boldsymbol{\varphi}}^+ + \bar{\boldsymbol{\varphi}}^-), \quad \tilde{\mathbf{t}} = \frac{1}{2}(\mathbf{t}^+ + \mathbf{t}^-) \tag{6}$$

The interface allows for displacement jumps across the two sides of the crease

$$[\![\mathbf{u}]\!] = \mathbf{u}^+ - \mathbf{u}^- = [\![\bar{\mathbf{u}}]\!] + \xi^3[\![\mathbf{t}]\!] \tag{7}$$

Equilibrium of the shell structure is imposed in weak form as

$$\delta\Pi_{\text{int}} - \delta\Pi_{\text{ext}} = 0 \tag{8}$$

where

$$\begin{aligned}\delta\Pi_{\text{ext}} &= \int_V \mathbf{b}\cdot\delta\mathbf{u}dV + \int_{\partial V}\mathbf{f}\cdot\delta\mathbf{u}dS\\ \delta\Pi_{\text{int}} &= \delta\Pi_{\text{int},V} + \delta\Pi_{\text{int},c} = \delta\Pi_{\text{int},V} + \int_{\Gamma_c}\int_{-\frac{t}{2}}^{\frac{t}{2}}\mathbf{P}\cdot\delta\mathbf{w}\mu d\xi^3 d\Gamma_c\end{aligned} \tag{9}$$

In Eq. (9), V is the volume occupied by the shell body in the reference configuration, ∂V is the portion of the boundary where traction boundary conditions are prescribed, $\mathbf{b}$ and $\mathbf{f}$ denote the assigned body and traction forces, respectively, $\delta\Pi_{\text{int},V}$ is the virtual internal work carried out in the shell body $V\setminus\Gamma_c\times\left[-\frac{t}{2},\frac{t}{2}\right]$, $\mathbf{P}dS$ is the internal force, due to the interface deformation, acting on the elementary area dS of the undeformed interface reference surface $\Gamma_c\times\left[-\frac{t}{2},\frac{t}{2}\right]$, μ accounts for the curvature of the crease reference line so that

$$\int_{\Gamma_c\times\left[-\frac{t}{2}\frac{t}{2}\right]}\mathbf{P}dS = \int_{\Gamma_c}\int_{-\frac{t}{2}}^{\frac{t}{2}}\mathbf{P}\mu d\xi^3 d\Gamma_c \tag{10}$$

and $\delta\mathbf{w}$ denotes the interface strain variation, conjugate to $\mathbf{P}$, which will be defined below. The variation $\delta[\![\mathbf{u}]\!]$ of the displacement jump in (7) is defined as

$$\delta[\![\mathbf{u}]\!] = \delta[\![\bar{\mathbf{u}}]\!] + \xi^3\delta[\![\mathbf{t}]\!] \tag{11}$$

and requires the definition of the virtual director jump $\delta[\![\mathbf{t}]\!]$. In view of the director inextensibility, the variation $\delta\mathbf{t}$ can be expressed as

$$\delta\mathbf{t} = \delta\vartheta\times\mathbf{t} \tag{12}$$

where $\delta\vartheta$ denotes a virtual rotation of the director $\mathbf{t}$ in the current configuration around an axis belonging to the plane orthogonal to $\mathbf{t}$. The virtual director jump $\delta[\![\mathbf{t}]\!]$ is then defined as:

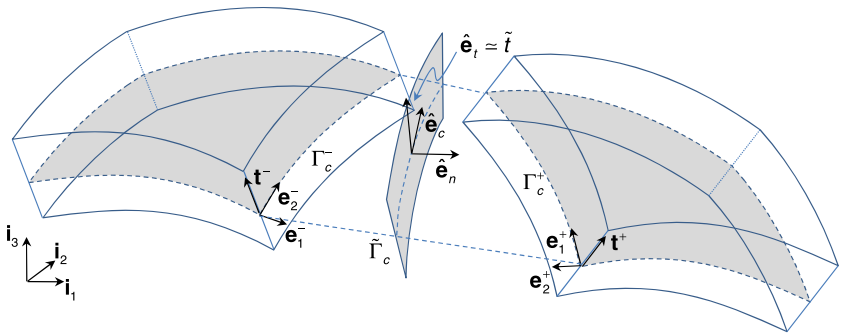

Fig. 6. Interface reference surface.

$$\delta[\![\mathbf{t}]\!] = \delta\mathbf{t}^+ - \delta\mathbf{t}^- = \delta\boldsymbol{\vartheta}^+ \times \mathbf{t}^+ - \delta\boldsymbol{\vartheta}^- \times \mathbf{t}^- = \delta[\![\boldsymbol{\vartheta}]\!] \times \tilde{\mathbf{t}} + \delta\tilde{\boldsymbol{\vartheta}} \times [\![\mathbf{t}]\!] \tag{13}$$

where $\delta\tilde{\boldsymbol{\vartheta}} = \frac{1}{2}(\delta\boldsymbol{\vartheta}^+ + \delta\boldsymbol{\vartheta}^-)$ and $\tilde{\mathbf{t}}$ is defined in Eq. (6)$_2$. Hence,

$$\delta[\![\mathbf{u}]\!] = \delta[\![\bar{\mathbf{u}}]\!] + \xi^3\delta[\![\boldsymbol{\vartheta}]\!] \times \tilde{\mathbf{t}} + \xi^3\delta\tilde{\boldsymbol{\vartheta}} \times [\![\mathbf{t}]\!] \tag{14}$$

As discussed in Giampieri and Perego (2011), the above definition of $\delta[\![\mathbf{u}]\!]$ contains a rigid rotation $\delta[\![\mathbf{u}]\!]^r = \delta\tilde{\boldsymbol{\vartheta}} \times [\![\bar{\mathbf{u}}]\!] + \xi^3\delta\tilde{\boldsymbol{\vartheta}} \times [\![\mathbf{t}]\!]$ of the interface, which may be not negligible when the crease opening becomes large. A pure opening mode $\delta\mathbf{w}$ of the interface is obtained from (14) by subtracting $\delta[\![\mathbf{u}]\!]^r$, i.e.

$$\delta\mathbf{w} = \delta\boldsymbol{\eta} + \xi^3\delta[\![\boldsymbol{\vartheta}]\!] \times \tilde{\mathbf{t}} \tag{15}$$

where $\delta\boldsymbol{\eta}$ is defined as

$$\delta\boldsymbol{\eta} = \delta[\![\bar{\mathbf{u}}]\!] - \delta\tilde{\boldsymbol{\vartheta}} \times [\![\bar{\mathbf{u}}]\!] \tag{16}$$

With these definitions, the virtual internal work in (9) is rewritten as

$$\delta\Pi_{\mathrm{int},c} = \int_{\Gamma_c} \mathbf{N} \cdot \delta\boldsymbol{\eta} d\Gamma_c + \int_{\Gamma_c} \mathbf{M} \cdot \delta[\![\boldsymbol{\vartheta}]\!] d\Gamma_c \tag{17}$$

where

$$\mathbf{N} = \int_{-\frac{t}{2}}^{\frac{t}{2}} \mathbf{P}\mu d\xi^3; \quad \mathbf{M} = \int_{-\frac{t}{2}}^{\frac{t}{2}} (\tilde{\mathbf{t}} \times \mathbf{P})\xi^3\mu d\xi^3 \tag{18}$$

are the generalized internal forces, work conjugate to the generalized strains $\delta\boldsymbol{\eta}$ and $\delta[\![\boldsymbol{\vartheta}]\!]$. For the definition of the constitutive behaviour of the interface, it is convenient to introduce at points on $\tilde{\Gamma}_c$ a local co-rotational orthogonal reference frame $\{\hat{\mathbf{e}}_c, \hat{\mathbf{e}}_t, \hat{\mathbf{e}}_n\}$ defined as (see Fig. 6)

$$\hat{\mathbf{e}}_c = \frac{\tilde{\mathbf{a}}_c}{\|\tilde{\mathbf{a}}_c\|}, \quad \hat{\mathbf{e}}_n = \tilde{\mathbf{a}}_n, \quad \hat{\mathbf{e}}_t = \hat{\mathbf{e}}_n \times \hat{\mathbf{e}}_c \tag{19}$$

where the tangent direction $\tilde{\mathbf{a}}_c$ to the deformed interface line $\tilde{\Gamma}_c$ and the unit normal vector $\tilde{\mathbf{a}}^n = \tilde{\mathbf{a}}_n$ are defined as

$$\tilde{\mathbf{a}}_c = \tilde{\boldsymbol{\varphi}}_{,\alpha}\partial\xi^\alpha/\partial\zeta, \quad \tilde{\mathbf{a}}^n = \frac{\tilde{\mathbf{a}}_c \times \tilde{\mathbf{t}}}{\|\tilde{\mathbf{a}}_c \times \tilde{\mathbf{t}}\|} = \tilde{\mathbf{a}}_n \tag{20}$$

Since large rotations are expected only around $\tilde{\mathbf{a}}_c$, $\hat{\mathbf{e}}_t$ and $\tilde{\mathbf{t}}$ are expected to remain almost parallel throughout the interface deformation process. The components of the generalized forces per unit length in the co-rotational basis are therefore given by (see Fig. 7):

$$V_c = \mathbf{N} \cdot \hat{\mathbf{e}}_c, \quad N = \mathbf{N} \cdot \hat{\mathbf{e}}_n, \quad V_t = \mathbf{N} \cdot \hat{\mathbf{e}}_t \tag{21}$$

$$M_c = \mathbf{M} \cdot \hat{\mathbf{e}}_c, \quad M_n = \mathbf{M} \cdot \hat{\mathbf{e}}_n, \quad M_t = \mathbf{M} \cdot \hat{\mathbf{e}}_t \simeq \mathbf{M} \cdot \tilde{\mathbf{t}} = 0 \tag{22}$$

where N is the normal force to the reference interface surface, V_c and V_t are the components of the shear force $\mathbf{V} = (\mathbf{I} - \hat{\mathbf{e}}_n \otimes \hat{\mathbf{e}}_n) \cdot \mathbf{N}$, M_c is the bending moment around the interface axis, M_n is the torque around the normal axis and the drilling moment M_t is taken equal to zero as discussed above.

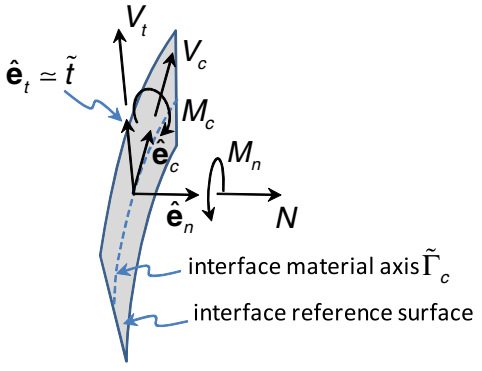

Fig. 7. Co-rotational components of internal forces and couples.

The generalized strains $\delta\boldsymbol{\eta}$ and $\delta[\![\boldsymbol{\vartheta}]\!]$ are similarly projected onto the co-rotational axes to obtain the kinematic quantities conjugated to the generalized forces and couples

$$\delta\eta_n = \delta\boldsymbol{\eta} \cdot \hat{\mathbf{e}}_n, \quad \delta\eta_c = \delta\boldsymbol{\eta} \cdot \hat{\mathbf{e}}_c, \quad \delta\eta_t = \delta\boldsymbol{\eta} \cdot \hat{\mathbf{e}}_t$$
$$\delta\vartheta_n = \delta[\![\boldsymbol{\vartheta}]\!] \cdot \hat{\mathbf{e}}_n, \quad \delta\vartheta_c = \delta[\![\boldsymbol{\vartheta}]\!] \cdot \hat{\mathbf{e}}_c$$

With this notation, the internal work is written as

$$\delta\Pi_{\mathrm{int},c} = \int_{\Gamma_c} [N\delta\eta_n + V_c\delta\eta_c + V_t\delta\eta_t + M_n\delta\vartheta_n + M_c\delta\vartheta_c] d\Gamma_c \tag{23}$$

4. Crease interface constitutive model

The paperboard is here considered as an elastic medium with inelastic dissipation localized in the crease interface. The interface constitutive law is expressed in terms of the generalized stresses and strains defined in the previous section in the interface co-rotational reference frame. The model will therefore represent the behavior of a section of unit width of the interface, as it is after the creasing process, i.e. for an assigned value of the nominal initial shearing strain γ.

As discussed in Section 2, when folding tests are performed on shallow-indented crease lines, a softening post-peak branch is observed in the bending response, while for deep-indented crease lines, perfect-plasticity can be regarded as the dominant dissipative mechanism. Therefore, since small deformations are expected in directions other than around the interface axis, unlimited and uncoupled linear elasticity is assumed for the shear sliding η_c, η_t and for the torque rotation ϑ_n, while a coupled damage-elastoplastic response is postulated for the membrane-bending deformation η_n, ϑ_c around the interface axis.

The constitutive model is formulated starting from the definition of a Helmoltz free energy density potential ${}^\gamma\Psi$ (where the superscript γ on the left of the symbol means that reference is made to a crease line obtained by a creasing process of intensity γ) in the form

$${}^\gamma\Psi = \frac{1}{2}k_c\eta_c^2 + \frac{1}{2}k_t\eta_t^2 + \frac{1}{2}k_n^+\langle\eta_n - \eta_n^p\rangle_+^2 + \frac{1}{2}{}^\gamma k_n^-\langle\eta_n - \eta_n^p\rangle_-^2 + \frac{1}{2}(1-d){}^\gamma k_{\vartheta_c}(\vartheta_c - \vartheta_c^p)^2 + \frac{1}{2}k_{\vartheta_n}\vartheta_n^2 \tag{24}$$

where k_i, $i = c, t, \vartheta_n$ denotes the generalized elastic stiffness, ${}^\gamma k_{\vartheta_c}$ and ${}^\gamma k_n^-$ denote the elastic bending and membrane compression stiffnesses which are assumed to be affected by the preceding creasing process, the superscript p denotes the plastic part of the generalized strains and the symbols $\langle\cdot\rangle_+$ and $\langle\cdot\rangle_-$ denote the positive and negative parts, respectively, of the contained quantity. Different elastic stiffnesses k_n^+ and ${}^\gamma k_n^-$ have been adopted for the membrane behavior in tension and compression, according to the experimental evidences. Additive decomposition in the co-rotational frame of elastic and plastic strains has been implicitly assumed in (24). It is worth remarking once more that the elastic stiffnesses k_i represent the generalized stiffnesses of the creased material as it results after it has been damaged in the creasing process. In the same way, the plastic strains due to folding are additional with respect to those generated during creasing, which are not considered here in an explicit way.

The linear elastic relations between the generalized static and kinematic quantities are obtained through the state equations of ${}^\gamma\Psi$ (see e.g. Lemaitre and Chaboche, 1994)

$$V_c = \frac{\partial^\gamma \Psi}{\partial \eta_c} = k_c \eta_c; \quad V_t = \frac{\partial^\gamma \Psi}{\partial \eta_t} = k_t \eta_t;$$
$$N = \frac{\partial^\gamma \Psi}{\partial \langle \eta_n - \eta_n^p \rangle_+} + \frac{\partial^\gamma \Psi}{\partial \langle \eta_n - \eta_n^p \rangle_-} = k_n^+ \langle \eta_n - \eta_n^p \rangle_+ + {}^\gamma k_n^- \langle \eta_n - \eta_n^p \rangle_-$$
$$M_c = \frac{\partial^\gamma \Psi}{\partial (\vartheta_c - \vartheta_c^p)} = (1-d)^\gamma k_{\vartheta_c} (\vartheta_c - \vartheta_c^p); \quad M_n = \frac{\partial^\gamma \Psi}{\partial \vartheta_n} = k_{\vartheta_n} \vartheta_n \tag{25}$$

The thermodynamic force conjugate to the damage variable is defined as

$$Y = -\frac{\partial^\gamma \Psi}{\partial d} = \frac{1}{2} {}^\gamma k_{\vartheta_c} (\vartheta_c - \vartheta_c^p)^2 \tag{26}$$

The dissipation rate density is therefore given by

$$\mathcal{D} = N \dot{\eta}_n^p + M_c \dot{\vartheta}_c^p + Y \dot{d} \geqslant 0 \tag{27}$$

4.1. Elastoplastic model

The crease region plastic response is formulated in the generalized stress effective space according to the hypothesis of strain equivalence (Lemaitre and Chaboche, 1994) and concerns the membrane-bending crease behavior only. Effective stresses are denoted by a superposed bar and are defined as

$$\overline{M}_c = \frac{M_c}{1-d}; \quad \overline{N} = N \tag{28}$$

Since the crease element allows for large membrane displacement jumps across the interface, membrane-bending coupling is accounted for in the definition of the yield criterion. Inelastic stress redistribution across the element thickness is however neglected, with a sharp transition from a purely elastic state to a fully plastic regime. This is motivated by the fact that the pre-peak behavior of the crease response is dominated by the progression of damage, as it will be discussed in the next subsection.

Denoting by $\sigma_y^+ > 0$ and $\sigma_y^- < 0$ the material yield limits in tension and in compression, respectively, the limit membrane forces N_y^+ and ${}^\gamma N_y^-$, their ratio $r > 0$ and the limit bending moment M_y are defined as

$$N_y^+ = \sigma_y^+ h, \quad {}^\gamma N_y^- = {}^\gamma N_y^- (\sigma_y^- h, \gamma), \quad r = -{}^\gamma N_y^- / N_y^+,$$
$$M_y = -\frac{t}{2} \frac{N_y^+ {}^\gamma N_y^-}{N_y^+ - {}^\gamma N_y^-} \tag{29}$$

It should be noted that in (29), the limit compression force ${}^\gamma N_y^-$ is assumed to be affected by the severity γ of the preliminary creasing operation. This aspect will be discussed in depth in Section 5.1.

For notation convenience, it is useful to introduce the nondimensional variables

$$n = \frac{\overline{N}}{N_y^+}, \quad m = \frac{\overline{M}_c}{M_y} \tag{30}$$

With this notation, the interface material elastic domain is assumed to be defined by the conditions (Fig. 8)

$$f_1(n,m) = \frac{n^2}{r} - \frac{1-r}{r} n + m - 1 \leqslant 0 \tag{31}$$
$$f_2(n,m) = \frac{n^2}{r} - \frac{1-r}{r} n - m - 1 \leqslant 0 \tag{32}$$

The generalized plastic strain rates $\dot{\eta}_n^p$ and $\dot{\vartheta}_c^p$ are defined according to an associated flow rule as

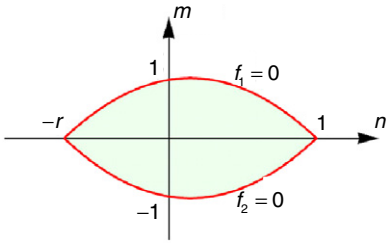

Fig. 8. Interface material elastic domain in m–n plane.

$$\dot{\eta}_n^p = \frac{\partial f_1}{\partial \overline{N}} \dot{\lambda}_1 + \frac{\partial f_2}{\partial \overline{N}} \dot{\lambda}_2 = \frac{1}{N_y^+} \left(\frac{\partial f_1}{\partial n} \dot{\lambda}_1 + \frac{\partial f_2}{\partial n} \dot{\lambda}_2 \right) \tag{33}$$
$$\dot{\vartheta}_c^p = \frac{\partial f_1}{\partial \overline{M}_c} \dot{\lambda}_1 + \frac{\partial f_2}{\partial \overline{M}_c} \dot{\lambda}_2 = \frac{1}{M_y} \left(\frac{\partial f_1}{\partial m} \dot{\lambda}_1 + \frac{\partial f_2}{\partial m} \dot{\lambda}_2 \right) \tag{34}$$

where $\dot{\lambda}_1$ and $\dot{\lambda}_2$ are nonnegative plastic multipliers, defined by the Kuhn–Tucker loading–unloading conditions

$$f_1 \leqslant 0, \quad f_2 \leqslant 0, \quad \dot{\lambda}_1 \geqslant 0, \quad \dot{\lambda}_2 \geqslant 0, \quad f_1 \dot{\lambda}_1 = f_2 \dot{\lambda}_2 = 0 \tag{35}$$

The backward-difference time-integration and the derivation of the consistent tangent moduli can be carried out following a standard approach and are not discussed here. Details of the derivation can be found in Giampieri and Perego (2011).

4.2. Damage model

The damage variable d in (24) is related to the development of delamination inside the creased region during folding. The creasing operation produces an initial damage in the creased material, nucleating defects and producing permanent deformation. During folding, the stress developing in the compressed side of the interface promotes buckling delamination of the compressed layers, facilitated by the presence of the pre-existing defects. Adopting a mesoscopic point of view (Fig. 9), damage can be thought of as a progressive reduction of the bending stiffness, due to the propagation of delamination through the interface thickness, departing from the compressed side.

Let the initially compact interface section of thickness t be imagined as composed of n_ℓ initially joined layers of equal thickness $t_i = t/n_\ell$. Let m_ℓ be the number of delaminated layers due to buckling. A mesoscopic damage indicator d^{meso} can be defined as the ratio between the numbers of buckled and total layers

$$d^{\text{meso}} = \frac{m_\ell}{n_\ell} \tag{36}$$

Delaminated layers contribute to the sectional bending stiffness in an additive way, and the sectional moment of inertia of the partially delaminated section is given by

$$I_c = \frac{1}{12} t_i^3 m_\ell + \frac{1}{12} [t_i (n_\ell - m_\ell)]^3 = I_c^0 \left[\frac{d^{\text{meso}}}{n_\ell^2} + (1 - d^{\text{meso}})^3 \right] \tag{37}$$

where $I_c^0 = 1/12\, t^3$ is the moment of inertia of the compact section. This corresponds to a highly simplified view of the phenomena

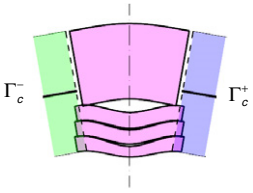

Fig. 9. Mesoscopic view of delaminating crease region.

occurring through the thickness during folding, since the progression of delamination in the longitudinal direction is not accounted for, as much as the possible contact between delaminated layers. Since the layer structure is not clearly defined through the crease thickness and, as it can be observed from Fig. 4, damage can develop anywhere in the interface thickness, a better description is obtained considering an infinite number of layers of vanishing thickness

$$I_c = \lim_{n_\ell \to \infty} I_c^0 \left[\frac{d^{\text{meso}}}{n_\ell^2} + (1 - d^{\text{meso}})^3 \right] = (1 - d^{\text{meso}})^3 I_c^0 = (1 - d) I_c^0 \quad (38)$$

where

$$d = (d^{\text{meso}})^3 - 3(d^{\text{meso}})^2 + 3 d^{\text{meso}} \quad (39)$$

is the macroscopic damage variable introduced in (24).

The evolution of the macroscopic damage is promoted by the shortening of the compressed layers. An equivalent measure of the effective compressive strain can be defined as

$$\varepsilon_{eq} = \frac{t}{2} (\vartheta_c^e + \vartheta_c^{p-} + \vartheta_c^{p+}) - c \eta_n \quad (40)$$

where ϑ_c^e is the elastic part of the crease rotation, ϑ_c^{p-} and ϑ_c^{p+} are the modules of the cumulated positive and negative parts of the plastic rotation and c is a material parameter. ϑ_c^{p-} and ϑ_c^{p+} are permanent strains and their effects do not cancel out when loading is reversed. $(-\eta_n)$ is the membrane shortening of the crease, which also contributes to the damage growth by increasing the lateral deflection of the buckled layers.

The damage evolution law is then defined as

$$\dot{d}^{\text{meso}} = \begin{cases} {}^{\gamma}a \dot{\varepsilon}_{eq} & \text{if } \varepsilon_{eq} > \bar{\varepsilon}_{eq},\ \dot{\varepsilon}_{eq} \geqslant 0 \quad \text{and } d^{\text{meso}} \leqslant d_{\text{lim}}^{\text{meso}} \\ 0 & \text{otherwise} \end{cases} \quad (41)$$

where ${}^{\gamma}a$ is a material parameter affected by the initial degree of creasing,

$$\bar{\varepsilon}_{eq}(t) = \max_{\tau \leqslant t} \varepsilon_{eq}(\tau) \quad (42)$$

is the maximum value attained by the equivalent strain during the crease deformation and $d_{\text{lim}}^{\text{meso}} \leqslant 1$ defines the maximum level of damage which can be reached within the crease section. The existence of an upper bound follows from the fact that sectional damage is promoted by layers compression which, during bending, has to be confined below the neutral axis and cannot extend throughout the section. The mesoscopic limit damage $d_{\text{lim}}^{\text{meso}}$ can be expressed in terms of the corresponding macroscopic quantity d_{lim}, which can be obtained measuring the residual bending stiffness in experimental tests on creased laminates, by means of Eq. (39)

$$d_{\text{lim}}^{\text{meso}} = 1 + \sqrt[3]{d_{\text{lim}} - 1} \quad (43)$$

Summarizing, the crease behavior is defined by the six elastic stiffness parameters $k_c, k_t, k_n^+, {}^{\gamma}k_n^-, {}^{\gamma}k_{\vartheta_c}, k_{\vartheta_n}$, the two membrane elastic limits N_y^+ and ${}^{\gamma}N_y^-$, obtainable from tension and compression membrane tests on the creased paperboard, and by the three damage parameters c, ${}^{\gamma}a$ and d_{lim}, obtainable from bending tests.

4.3. Dissipation inequality check

The second principle of thermodynamics requires that the dissipation rate (27) is nonnegative for all possible deformation processes. Substituting in (27) the expressions (33) and (34) for $\dot{\eta}_n^p$ and $\dot{\vartheta}_c^p$, one can write

$$\mathcal{D} = \left(\frac{2n^2}{r} - \frac{1-r}{r} n + (1-d) m \right) \dot{\lambda}_1 + \left(\frac{2n^2}{r} - \frac{1-r}{r} n - (1-d) m \right) \dot{\lambda}_2 + Y \dot{d} \geqslant 0 \quad (44)$$

When damage is zero, the inequality is certainly satisfied because the plastic model satisfies Drucker's postulate. When both damage and plasticity are active, a sufficient condition for (27) to hold can be sought as follows.

First of all, let us discard the always nonnegative term $Y\dot{d}$. In the case that both $\dot{\lambda}_1 \geqslant 0$ and $\dot{\lambda}_2 \geqslant 0$, the vertex on the $m = 0$ axis is active. But if $m = 0$, the contribution of damage to (44) vanishes and, again, the inequality is satisfied.

Let us consider then the case $\dot{\lambda}_1 \geqslant 0,\ f_1 = 0,\ \dot{\lambda}_2 = 0$ (the case $\dot{\lambda}_2 \geqslant 0,\ f_2 = 0, \dot{\lambda}_1 = 0$ can be treated in a similar way). In this case, exploiting the fact that m can be eliminated using the condition $f_1 = 0$, the sufficient condition can be written as

$$\left[1 + \frac{n^2}{r} - d \left(1 - \frac{n^2}{r} + \frac{1-r}{r} n \right) \right] \dot{\lambda}_1 \geqslant 0 \quad (45)$$

and hence, in view of the nonnegativeness of $\dot{\lambda}_1$,

$$d \leqslant \frac{1 + \frac{n^2}{r}}{1 - \frac{n^2}{r} + \frac{1-r}{r} n} \quad (46)$$

A sufficient condition can be found imposing that

$$d \leqslant \min_n \left(\frac{1 + \frac{n^2}{r}}{1 - \frac{n^2}{r} + \frac{1-r}{r} n} \right) \quad (47)$$

For $r = 1$ (equal yield limits in tension and compression), one obtains that the r.h.s. in (47) is equal to 1, leading to the trivial condition $d \leqslant 1$. This would mean that the sufficient condition is always satisfied. The r.h.s. of (47) is an increasing function of r. E.g., for $r = 1/10$ one obtains the condition $d \leqslant 0.58$. In the proposed model, damage is bounded to be not greater than the limit damage d_{lim}, which is a constitutive parameter. The condition (47) can be replaced therefore by the condition

$$d_{\text{lim}} \leqslant \min_n \left(\frac{1 + \frac{n^2}{r}}{1 - \frac{n^2}{r} + \frac{1-r}{r} n} \right) \quad (48)$$

which turned out to be satisfied in all the practical cases considered in the present work.

5. Creasing process effects on interface behavior

5.1. Effects on elastic and plastic parameters

The creasing process produces a degradation of the paperboard elastic stiffness and strength. This degradation is due to the combined effects of the propagation of damage delamination, through the width W of the creased region (W being the width of the channel die defined in (1)) and through the paperboard thickness t, and to the geometric effects produced by the permanent deflection. Depending on the intensity γ of the creasing, a more or less significant permanent out-of-plane deflection is observed after creasing, which boosts the buckling of compressed delaminated layers during bending.

Several micro and meso-mechanical models have been proposed in the literature (Xia et al., 2002; Nygårds et al., 2005; Beex and Peerlings, 2009) to simulate damage propagation during the creasing process. These gave rise to accurate 3D numerical models, which however appear to be unsuitable for large scale computations of whole packages. A different point of view, at the

meso-scale level, was adopted by Carlsson et al. (1983) to capture the basic feature of the bending behavior of the creased paperboard. In their model, two parallel beams, connected to each other at their ends, are bent together. The beam on the compressed side is given an initial deflection (accounting for the creasing permanent deformation) and buckles under compression, while the other beam elongates in tension. The point of view adopted in this work is inspired by Carlsson et al. (1983) model, even though a purely phenomenological approach is followed here. Based on the observation of the physical processes taking place during creasing, it is assumed that:

- both strength and stiffness of the crease line deteriorate during creasing, proportionally to the intensity of the creasing process, measured by the nominal initial shearing strain γ defined in Eq. (1);
- a greater penetration depth (higher γ) of the indenter during creasing has the following two main effects: (i) the formation of thinner delaminated layers; (ii) a greater permanent out-of-plane deflection (Fig. 10a);
- the deterioration of mechanical properties is a consequence of the increasing slenderness, driven by the thickness reduction, and of the permanent out-of-plane deflection of the delaminated layers.

The attention is now focused on a typical delamination layer, of thickness ${}^{\gamma}t$, generated by a creasing process of intensity γ which is compressed during paperboard folding, occurring after creasing. During folding, the compressed delaminated layer is assumed to behave as the beam in Fig. 10b, of unit width, of length W, equal to the width of the channel die, and with initial deflection h, equal to the indentation depth (see Fig. 1). The initial deflected shape is expressed as

$$\bar{v}(x) = \frac{h}{2}\left[\cos\frac{2\pi x}{W} - 1\right] \tag{49}$$

Adopting a linearized theory, the beam elastic deflection due to the application of a compression axial force P is then given by

$$v(x) = \frac{1}{1-\frac{P}{P_E}}\bar{v}(x) \tag{50}$$

where

$$P_E = \frac{4\pi^2 E^{\gamma} I}{W^2} \tag{51}$$

is the Eulerian buckling load, ${}^{\gamma}I = 1/12\,{}^{\gamma}t^3$ being the layer moment of inertia. The bending moment (assumed positive for the deflected shape in Fig. 10b) at the beam midspan is given by

$$M_c\left(\frac{W}{2}\right) = \frac{1}{1-\frac{P}{P_E}}\frac{h}{2}P \tag{52}$$

Defining the beam slenderness χ as

$$\chi^2 = \frac{W^{2\gamma}t}{4^{\gamma}I} \tag{53}$$

the buckling load can be expressed as

$$P_E = \frac{\pi^2 E^{\gamma} t}{\chi^2} \tag{54}$$

Assuming for the present purposes that the layer material has symmetric elastic strength in tension and compression and setting $N = -P,\ N_E = -P_E,\ N_y^+ = -N_y^- = N_y = \sigma_y{}^{\gamma}t,\ \tilde{n} = N/N_y$, one can write

$$\frac{P}{P_E} = \frac{N}{N_E} = \frac{N}{N_y}\frac{N_y}{N_E} = -\tilde{n}\frac{\chi^2}{\chi_y^2} \quad \text{with } \chi_y^2 = \frac{\pi^2 E}{\sigma_y} \tag{55}$$

Substituting for P/P_E and P in (52) and taking into account that $M_y = N_y{}^{\gamma}t/4$ for the considered rectangular section, one has for $\tilde{n} < 0$ and $\chi \geqslant \chi_y$

$$\tilde{m}\left(\frac{W}{2}\right) = \left(\frac{M_c\left(\frac{W}{2}\right)}{M_y}\right) = -\frac{1}{1+\tilde{n}\frac{\chi^2}{\chi_y^2}}\frac{2h}{{}^{\gamma}t}\tilde{n} \quad \text{for } \chi \geqslant \chi_y \tag{56}$$

For $\chi < \chi_y$ the axial compression is assumed to have reached its plastic limit, independent of the geometric effect, and (56) does not hold.

According to a standard approach, the beam limit state is obtained for $\chi \geqslant \chi_y$ by assuming that the axial force and the bending moment reach the boundary of the elastic domain, defined in (31) with $r = 1$, in the most stressed section. Substituting (56) in (31) one has

$$\frac{\chi^2}{\chi_y^2}\tilde{n}^3 + \tilde{n}^2 - \left(\frac{\chi^2}{\chi_y^2} + \frac{2h}{t}\frac{t}{{}^{\gamma}t}\right)\tilde{n} - 1 = 0 \tag{57}$$

The values $\tilde{n}(\gamma)$ satisfying (57) are taken as effective current values of the yield limit in compression ${}^{\gamma}N_y^- = -\tilde{n}(\gamma)\,{}^{0}N_y^-$, with $\tilde{n}(0) = -1$, of the creased paperboard, where N_y^+ is the paperboard yield limit in tension, defined in (29), which is assumed to be unaffected by γ, and ${}^{0}N_y^-$ is the yield limit in compression of the uncreased paperboard. The corresponding limit bending moment ${}^{\gamma}M_y$ is obtained by means of $(29)_4$.

The penetration depth h in (57) is replaced by an effective value $\tilde{h}$ which, on the basis of Eq. (1), is expressed as

$$\frac{\tilde{h}}{t} = \begin{cases} 0 & \text{for } 0 \leqslant \gamma \leqslant \bar{\gamma} \\ \frac{W}{2t}(\gamma - \bar{\gamma}) & \text{for } \bar{\gamma} \leqslant \gamma \end{cases} \tag{58}$$

where $\bar{\gamma}$ is a limit value of the nominal shearing strain below which there is no geometric effect (e.g. because the imposed deflection is recovered upon unloading). The relation (58) can be expressed in regularized form as (see Fig. 11a for $W/t = 3.26$, and $\bar{\gamma} = 0.2$)

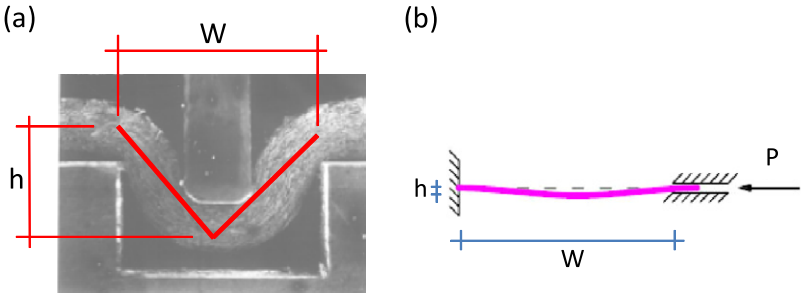

Fig. 10. (a) Effects on indentation depth during creasing. (b) Deflected beam model for compressed layer.

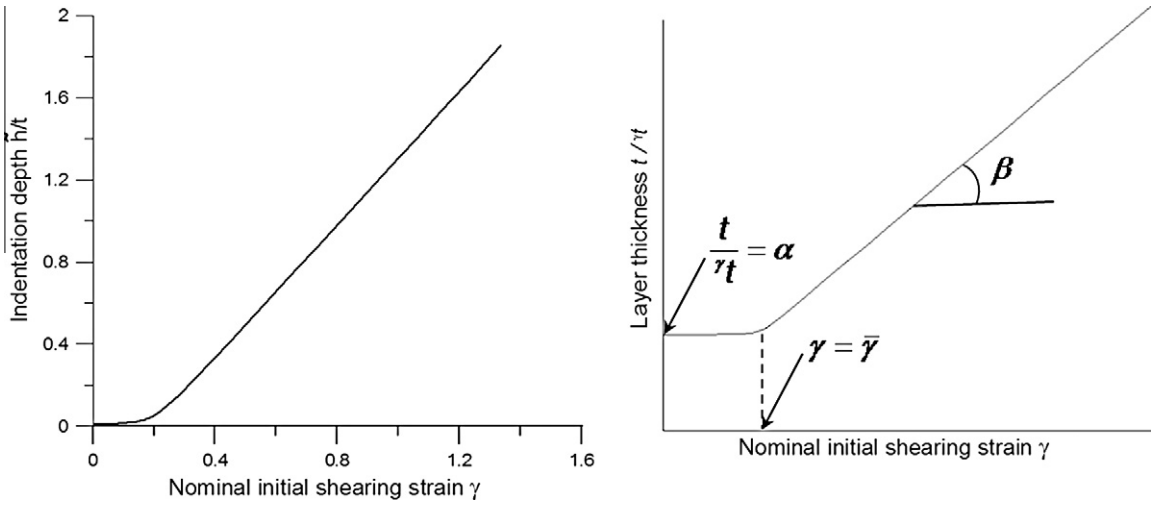

Fig. 11. Effects of nominal initial shearing strain γ: (a) effective indentation depth. (b) thickness ${}^{\gamma}t$ of compressed layer.

$$\frac{\tilde{h}}{t}=\frac{W}{4t}\left[(\gamma-\bar{\gamma})+\sqrt{(\gamma-\bar{\gamma})^2+4\kappa}\right] \tag{59}$$

κ being a sufficiently small regularization parameter (here it is taken $\kappa = 10^{-3}$).

In view of its definition (53), the slenderness χ can be expressed as

$$\chi=\sqrt{3}\frac{W}{t}\frac{t}{{}^{\gamma}t} \tag{60}$$

As previously mentioned, a creasing process of increasing severity produces thinner delaminated layers. Since for $\gamma \leqslant \bar{\gamma}$ the geometric effect in (57) is negligible, the ratio $t/{}^{\gamma}t$ in (60), between the paperboard and the delaminated layer thicknesses, is then taken to remain constant for $\gamma \leqslant \bar{\gamma}$ and to increase linearly with γ for $\gamma > \bar{\gamma}$, according to the empirical relation

$$\frac{t}{{}^{\gamma}t}=\frac{1}{2}\left[\beta(\gamma-\bar{\gamma})+2\alpha+\sqrt{[\beta(\gamma-\bar{\gamma})+2\alpha]^2-4\alpha[\beta(\gamma-\bar{\gamma})+\alpha]+4\kappa}\right] \tag{61}$$

depending on the two scalar parameters α and β (see Fig. 11). For $\gamma < \bar{\gamma}$, one has $t/{}^{\gamma}t = \alpha$. This is the limit situation of thick layer corresponding to a slenderness $\chi < \chi_y$. Hence, the parameter α is obtained imposing that $\chi = \chi_y$ for $t/{}^{\gamma}t = \alpha$, i.e.

$$\alpha=\frac{t}{W}\frac{\chi_y}{\sqrt{3}} \tag{62}$$

Replacing h in (57) with $\tilde{h}$ from (59) and $t/{}^{\gamma}t$ with its expression in (61), one obtains an implicit equation for $\tilde{n}$ as a function of γ, depending on the empiric parameters $\bar{\gamma}$ and β. For the particular geometry and material considered by Nagasawa et al. (2003) in their experimental tests and for $\bar{\gamma} = 0.2$ and $\beta = 1$, the solid curve shown in Fig. 12 is obtained (using a symbolic algebra manipulator) from Eq. (57), modified as mentioned above.

Since Eq. (57) cannot be given a simple explicit expression, the solid curve is approximated using a hyperbolic tangent function (dashed curve in Fig. 12)

$$\tilde{n}(\gamma)=\left(\frac{1-\tilde{n}(\gamma^{\max})}{2}\right)\tanh[g(\gamma)]+\left(\frac{1+\tilde{n}(\gamma^{\max})}{2}\right) \tag{63}$$

where

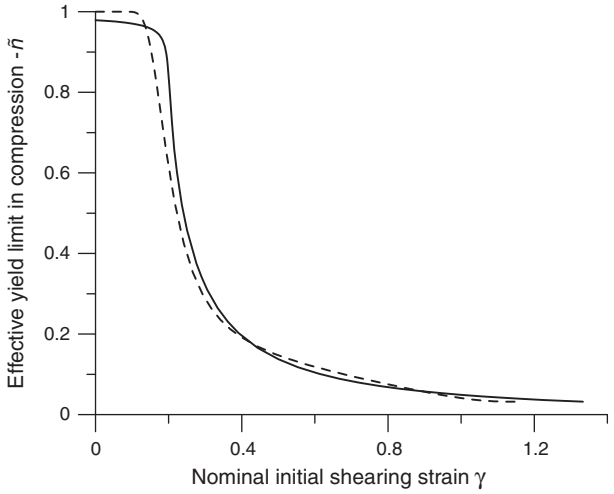

Fig. 12. Effects of nominal initial shearing strain γ on effective membrane compression strength $\tilde{n}(\gamma)$ (solid line). Hyperbolic tangent approximation (dashed line).

$$g(\gamma)=\left(\frac{\gamma^c}{\gamma}\right)^2-\sqrt{\frac{\gamma^c-\gamma^{\max}}{\gamma-\gamma^{\max}}} \tag{64}$$

is a function which scales γ from the interval $\gamma \in [0,\gamma^{\max}]$ to $g(\gamma) \in [0,\infty]$, and γ^c defines a center for the hyperbolic tangent. The result of the approximation for $\gamma^{\max} = 4/3$, $\gamma^c = 0.25$ and $\tilde{n}(\gamma^{\max}) = 0.13$ is given by the dashed curve in Fig. 12. The evolution of the elastic domain in the effective generalized stress plane $\overline{M}_c$–$\overline{N}$ is shown in Fig. 13.

The same type of dependence on the severity γ of the creasing is postulated also for the membrane and bending elastic stiffnesses.

$$\begin{aligned}{}^{\gamma}k_n^- &= \left(\frac{{}^{0}k_n^- - k_n^-(\gamma^{\max})}{2}\right)\tanh[q(\gamma)]+\left(\frac{{}^{0}k_n^- + k_n^-(\gamma^{\max})}{2}\right)\\ {}^{\gamma}k_{\vartheta_c} &= \left(\frac{{}^{0}k_{\vartheta_c} - k_{\vartheta_c}(\gamma^{\max})}{2}\right)\tanh[q(\gamma)]+\left(\frac{{}^{0}k_{\vartheta_c} + k_{\vartheta_c}(\gamma^{\max})}{2}\right)\end{aligned} \tag{65}$$

where

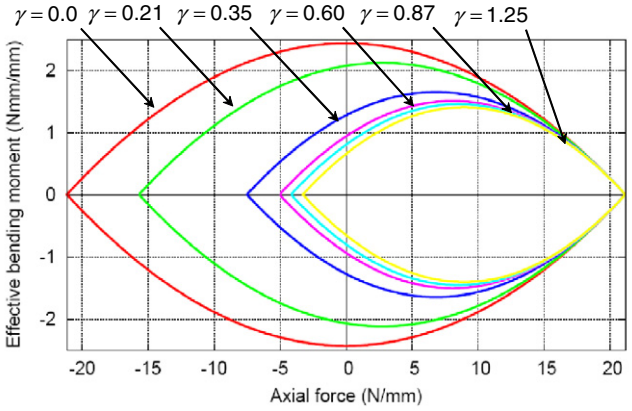

Fig. 13. Evolution of elastic domain in $\overline{M}$–$\overline{N}$ plane for growing initial nominal shearing strain γ.

$$q(\gamma) = \left(\frac{\gamma^c_{k_a}}{\gamma}\right) - \left(\frac{\gamma^c - \gamma^{\max}}{\gamma - \gamma^{\max}}\right) \tag{66}$$

is a scaling function and $\gamma^c_{k_a}$ $(a = n, \vartheta_c)$ has to be identified for each curve from a best fitting of experimental data.

5.2. Effects on damage behavior

The bending stiffness ${}^{\gamma}k_{\vartheta_c}$ decreases during the creasing process according to (65). When, after creasing, the paperboard is folded around the crease line, the bending stiffness further deteriorates due to damage growth, measured by the damage variable d in (24), which evolves according to (39) and (41) until the limit value $d_{\lim}$ is reached. $d_{\lim}$ represents the maximum fraction of the bending stiffness of the creased material which can be lost during folding and here it is assumed to be independent of the creasing intensity γ. On the other hand, the damage rate is not constant, as in pure bending it depends on the rotation rate around the crease line through the constant ${}^{\gamma}a$ in (41), which is affected by the creasing depth. To establish the dependence of ${}^{\gamma}a$ on the initial nominal shearing strain γ, let us consider the case of monotonic pure bending after creasing. According to (40) and (41), one has

$$d^{\text{meso}}_{\lim} = {}^{\gamma}a\frac{t}{2}\left({}^{\gamma}\vartheta_y + {}^{\gamma}\vartheta^p_{\lim}\right) \tag{67}$$

where ${}^{\gamma}\vartheta_y$ is the rotation corresponding to the attainment of the elastic limit and ${}^{\gamma}\vartheta^p_{\lim}$ is the subsequent plastic rotation corresponding to the achievement of the limit damage $d_{\lim}$. While ${}^{\gamma}\vartheta_y$ is easily obtained from the corresponding values of the limit bending moment ${}^{\gamma}M_y$ and bending stiffness ${}^{\gamma}k_{\vartheta_c}$, discussed in the previous section, as

$${}^{\gamma}\vartheta_y = \frac{{}^{\gamma}M_y}{{}^{\gamma}k_{\vartheta_c}} \tag{68}$$

the limit ${}^{\gamma}\vartheta^p_{\lim}$ needs some further discussion. As observed by Carlsson et al. (1983), in uncreased and shallow creased paperboard, there is experimental evidence that plastic strains start developing on the compression side before the peak moment resistance is reached. This suggests that the limit damage is attained when the crease material is already in the plastic range. On the contrary, for a deeply creased paperboard ($\gamma \geqslant \gamma^{\text{trans}} = 0.6$ in Fig. 5), where significant delamination has already taken place during creasing, no peak is observed in the moment-rotation curve, meaning that plasticity starts developing when damage has already reached its limit value and, hence, ${}^{\gamma}\vartheta^p_{\lim} = 0$ for $\gamma \geqslant \gamma^{\text{trans}}$. In view of this experimental evidences, it is here assumed that for deep creasing ($\gamma \geqslant \gamma^{\text{trans}}$) the damage limit is attained in pure bending for the rotation ${}^{\gamma}\vartheta_y$ corresponding to the elastic limit. The expression (67) modifies as

$$d^{\text{meso}}_{\lim} = \begin{cases} {}^{\gamma}a\frac{t}{2}{}^{\gamma}\vartheta_y\left(1 + \frac{{}^{\gamma}\vartheta^p_{\lim}}{{}^{\gamma}\vartheta_y}\right) & \text{for } \gamma < \gamma^{\text{trans}} \\ {}^{\gamma}a\frac{t}{2}{}^{\gamma}\vartheta_y & \text{for } \gamma \geqslant \gamma^{\text{trans}} \end{cases} \tag{69}$$

and hence

$${}^{\gamma}a = \begin{cases} \dfrac{d^{\text{meso}}_{\lim}}{\frac{t}{2}{}^{\gamma}\vartheta_y}\dfrac{1}{\left(1+\frac{{}^{\gamma}\vartheta^p_{\lim}}{{}^{\gamma}\vartheta_y}\right)} & \text{for } \gamma < \gamma^{\text{trans}} \\ \dfrac{d^{\text{meso}}_{\lim}}{\frac{t}{2}{}^{\gamma}\vartheta_y} & \text{for } \gamma \geqslant \gamma^{\text{trans}} \end{cases} \tag{70}$$

While ${}^{\gamma}\vartheta_y$ is defined in (68), for $\gamma < \gamma^{\text{trans}}$, ${}^{\gamma}\vartheta^p_{\lim}$ depends on the creasing depth γ and is a parameter to be identified by experimental tests. The value of ${}^{\gamma}\vartheta^p_{\lim}$ affects the damage rate through ${}^{\gamma}a$ and is a decreasing function of γ. In the numerical results presented in the next section, the following simple quadratic function of γ has been empirically adopted

$${}^{\gamma}\vartheta^p_{\lim} = {}^{0}\vartheta^p_{\lim}\left(1 - \frac{\gamma}{\gamma^{\text{trans}}}\right)^2 \tag{71}$$

where ${}^{0}\vartheta^p_{\lim}$ denotes the plastic rotation corresponding to the attainment of the limit damage during folding of an uncreased paperboard.

6. Numerical results

The proposed constitutive model has been implemented in a 2-node interface element based on the kinematic description of Section 3. The interface element is to be interposed between two adjacent 4-node shell finite elements. A complete discussion of the implementation can be found in Giampieri and Perego (2011). The crease interface element has been used for the simulation of the bending tests carried out by Nagasawa et al. (2003).

6.1. Numerical model description

A strip of paperboard of 60 mm (MD) ×40 mm (CD) ×0.46 mm (ZD) has been used for the tests and has been discretized by 4-node shell finite elements. As described in Section 2, part of the strip is secured to rotating clamps (Figs. 3 and 14). The element nodes in this region have been assigned a quasi-static motion along a circular trajectory, from $\Theta = 0°$ to $\Theta = 90°$ with rotation increments $\Delta\Theta = 0.5°$. A line of interface crease elements, aligned in cross-direction (CD) has been placed at the end of the constrained region (Fig. 14), while the ZD displacement of elements in contact with the load cell, aligned in CD at a distance of 25 mm from the crease line, is constrained to be zero. The ZD reaction forces at these nodes are used for the computation of the bending moment around the crease line. As it is clear from the description of the test setup, the test measures the response of the paperboard strip and not of the crease line. Several factors may contribute to make these responses different, such as the elastic curvature of the strip portion comprised between the clamps and the load cell (which is however

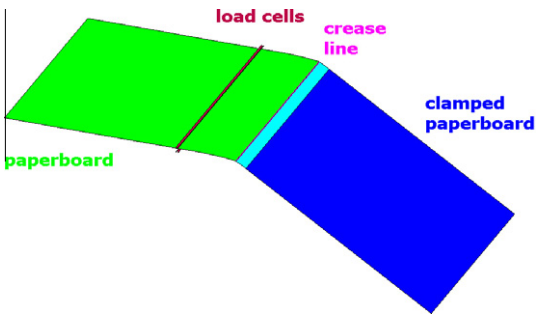

Fig. 14. Numerical model geometry.

easily discounted) and, most of all, a possible misalignment between the crease axis and the imposed rotation axis. As discussed by Nagasawa et al. (2003), this can be caused e.g. by misalignment of the indenting rule during the creasing process. However, from a visual inspection of the deformed shapes of the tested specimens in Fig. 4, all exhibiting a rotation substantially centered on the crease axis, one can conclude that the effects of misalignment on the results is negligible in the reported cases. The finite element analyses have been carried out under quasi-static conditions, adopting the Adaptive Dynamic Relaxation (ADR) incrementation strategy (Oakley and Knight, 1995a,b) as described in Giampieri and Perego (2011).

The experimental tests were carried out on three kinds of low quality white paperboard with slightly different tensile strength. A reference value of $\sigma_y = 46.0$ MPa, symmetric in tension and compression for the uncreased paperboard, has been used for the simulations. The authors do not report about the paperboard elastic properties, with the exception of the bending stiffness, whose degradation due to the creasing process has been measured. The other elastic stiffnesses of the crease line material have been found to have little influence on the bending behavior and have been assigned the values in Table 1, based on information from the literature. As for the membrane stiffness, symmetric tension–compression behavior has been assumed for the uncreased paperboard (i.e. ${}^0k_n^- = k_n^+$) while a 75% degradation of the compression stiffness has been assumed in correspondence of the maximum value $\gamma^{\max} = 1.7$ of the nominal shearing strain (i.e. $k_n^-(\gamma^{\max}) = 0.25\,{}^0k_n^-$). The parameter $\gamma^c_{k_n}$ for the definition of the hyperbolic tangent in $(65)_1$ has been taken as $\gamma^c_{k_n} = 0.3$. The bending stiffnesses for the uncreased and fully creased ($\gamma^{\max} = 1.7$) paperboard have been directly obtained from the experimental results provided by Nagasawa et al. (2003), while $\gamma^c_{k_{\vartheta_c}} = 0.6$ has been used in $(65)_2$ for the interpolation.

As for the parameters characterizing the damage behavior, $c = 0$ has been taken in (40), due to lack of experimental information on coupled membrane bending behavior, while the values ${}^0\vartheta^p_{\lim} = 15.7°$ in (71) and $d^{\text{meso}}_{\lim} = 0.4$ with a transition value $\gamma^{\text{trans}} = 0.6$ have been identified from the experimental results. A summary of the adopted material constants is reported in Table 1.

6.2. Simulation results

The bending test in Fig. 14 has been simulated for the six different values of the nominal initial shearing strain $\gamma = 0.0$, $\gamma = 0.21$, $\gamma = 0.35$, $\gamma = 0.6$, $\gamma = 0.87$, $\gamma = 1.25$, considered in the experimental tests documented in Nagasawa et al. (2003), corresponding to increasing severity of the preliminary creasing process. The experimental results already shown in Fig. 5 are plotted again in Fig. 15 together with the results of the corresponding finite element simulations, obtained using the material parameters in Table 1.

Good agreement can be observed as for the general trend of the crease response for varying γ. From the comparison of the numerical curves with the corresponding experimental curves, the following comments can be made:

- the main features of the transition for $\gamma = 0.6$ between shallow and deep indentation are well captured by the model;
- the softening post-peak branch due to damage in the shallow creasing range ($\gamma < 0.6$) is correctly reproduced;
- the limit value of the bending moment for $\vartheta_c \to 90°$ is accurately approximated for all considered values of γ;
- the quality of the approximation deteriorates for extreme values of γ ($\gamma \lessapprox 0.2$, $\gamma \gtrapprox 0.9$) while it appears to be quite satisfactory for the range of values of interest in practical applications.

The latter remark emphasizes the limitations of the proposed model, which is intrinsically macroscopic and accounts for events at the mesoscopic scale in a phenomenological way. For very low or very high creasing depth, complex phenomena, which necessitate a description at a lower scale, take place in the crease region as it can be clearly observed from the pictures in Fig. 4. For very shallow creasing, extensive damage occurs on the tensile side and the simple buckling beam model considered in Section 5.1 is not adequate to describe the wavy deformed shape on the compression side, visible in Fig. 4. For very deep creasing, delamination occurs throughout the paperboard depth and extends beyond the width of the initial creasing region. While these aspects are not included in the simple proposed model, the main features of the crease deformation in the middle range of γ values appear to be satisfactorily caught.

Fig. 16 shows the evolution with γ of: (a) the initial bending stiffness ${}^\gamma k_{\vartheta_c}$, (b) the peak bending moment at the crease interface and (c) the corresponding rotation angle, respectively. In both the first two cases, the quality of the approximation is very good. It should be noted that, while the trend of the initial bending stiffness is the results of the interpolation in Eq. $(65)_2$, the maximum bending moment depends on the evolution of the elastic domain (see Fig. 13) and on the interaction between the damage and plastic dissipation mechanisms. It is therefore an outcome of the constitutive model. In contrast, the experimental and numerical peak angles show good agreement only for $\gamma < \gamma^{\text{trans}} = 0.6$. This can be explained with the fact that for $\gamma > \gamma^{\text{trans}}$ the experimental curves in Fig. 15 do not exhibit a clearly distinguishable peak and the authors do not provide details on how the corresponding angle is identified. In the simulations, the peak angle for $\gamma > \gamma^{\text{trans}}$ is taken as the angle

Table 1
Material parameters for numerical model.

Test parameters			
$t = 0.46$ mm	$\gamma^{\min} = 0$	$\gamma^{\max} = 1.7$	$\gamma^{\text{trans}} = 0.6$
Elastic parameters			
$k_c = 100$ N/mm^2	$k_t = 100$ N/mm^2		
$k_n^+ = {}^0k_n^- = 2162.0$ N/mm^2			
$k_n^-(\gamma^{\max}) = 540.5$ N/mm^2	$\gamma^c_{k_n} = 0.3$		
${}^0k_{\vartheta_c} = 0.1$ N/deg			
$k_{\vartheta_c}(\gamma^{\max}) = 0.019$ N/deg	$\gamma^c_{k_{\vartheta_c}} = 0.6$		
Plastic parameters			
$N_y^+ = 21.16$ N/mm^2			
${}^0N_y^- = -21.16$ N/mm			
$N_y^-(\gamma^{\max}) = -2.75$ N/mm	$\gamma^c = 0.25$		
Damage parameters			
$c = 0$	${}^0\vartheta^p_{\lim} = 15.7°$	$d^{\text{meso}}_{\lim} = 0.4$	

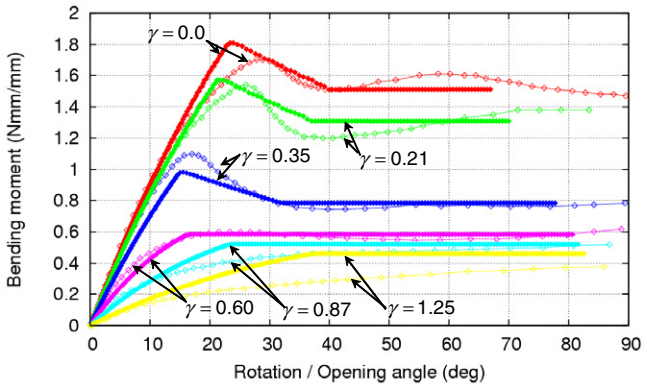

Fig. 15. Bending test: comparison between numerical and experimental results.

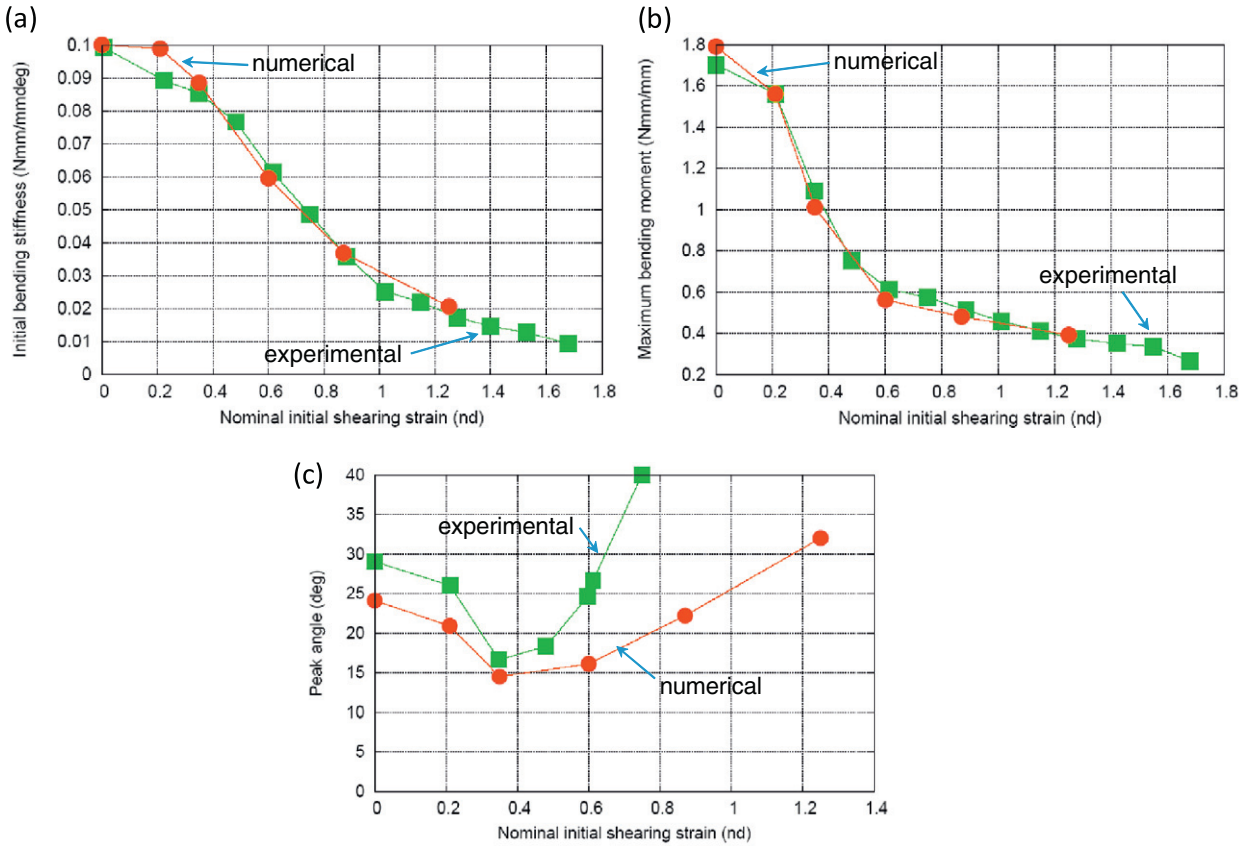

Fig. 16. Bending test. Evolution for varying nominal initial shearing strain γ: (a) initial bending stiffness; b) peak bending moment; (c) rotating angle at peak bending moment.

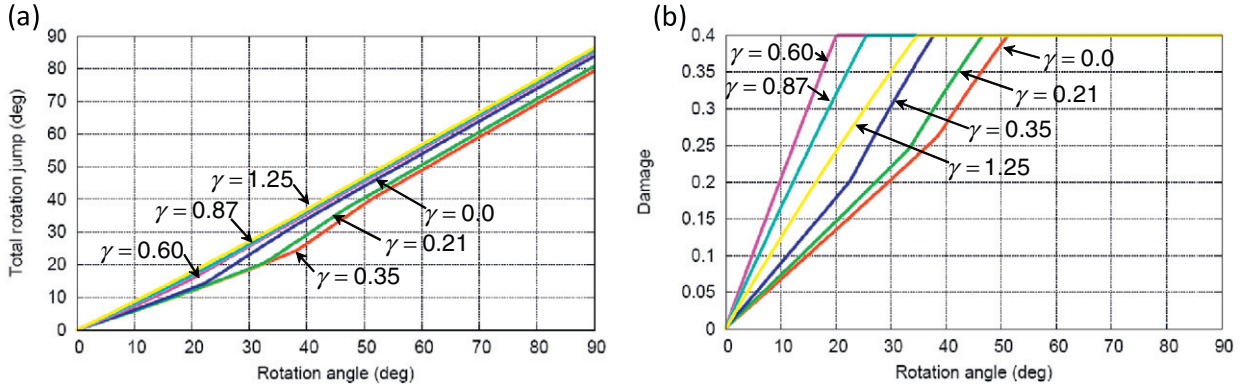

Fig. 17. Bending test. Evolution with imposed rotation angle Θ: (a) total crease rotation, (b) damage.

corresponding to the attainment of the limit damage $d_{\text{lim}}^{\text{meso}}$. For rotations larger than this angle, the interface response is perfectly plastic, with constant bending moment.

Fig. 17a shows the ratio between the total (elastic plus plastic) rotation jump ϑ_c at the crease interface and the rotation Θ applied to the clamps of the testing rig, for the different values of γ. As expected, for low γ one has $\vartheta_c < \Theta$, because of the elastic deformation of the paperboard outside the crease region. For $\gamma < \gamma^{\text{trans}}$, ϑ_c grows faster than Θ when the material enters the softening branch, due to strain localization occurring in the crease region, while elastic unloading is occurring outside. For increasing rotation angles, the interface behaves as a plastic hinge and one has $\dot{\vartheta}_c = \dot{\Theta}$. For $\gamma > \gamma^{\text{trans}}$, the difference between ϑ_c and Θ vanishes since the beginning, due to the reduction of the interface initial bending stiffness.

Fig. 17b shows the evolution of the damage variable d^{meso} with the imposed rotation angle Θ. As explained in Section 5.2, damage grows until the limit threshold is attained ($d_{\text{lim}}^{\text{meso}} = 0.4$ in these simulations, see Table 1). The damage rate varies with γ according to the coefficient ${}^{\gamma}a$ in (70). For $\gamma \leqslant \gamma^{\text{trans}}$, the damage rate increases significantly in correspondence of the activation of the plastic response. For $\gamma > \gamma^{\text{trans}}$, the activation occurs in correspondence of the limit damage and the damage rate remains constant with the rotation angle up to that point.

7. Conclusions

An interface finite element, to be interposed between adjacent shell elements, and its corresponding crease constitutive model

have been formulated for the modeling of the folding behavior of creased paperboard. The proposed interface element is intended to be used for the full-scale simulation of the forming process of carton packages and as a numerical tool for the optimization of the crease pattern design. For this reason, its main requisite is to be computationally inexpensive.

The proposed model, formulated in terms of generalized variables, is macroscopic and interprets in a phenomenological way the complex phenomena occurring at lower scales. For this reason, it requires only a relatively small number of parameters to be characterized and can be considered to be 'simple', especially if compared to other more accurate approaches proposed in the literature and based on the through-thickness discretization of the creased paperboard (Nygårds et al., 2009; Beex and Peerlings, 2009). The use of the simplified buckling beam approach of Section 5.1 provides a mechanical foundation for the interpretation of the dependence of the folding behavior on the initial shearing parameter and it allows, through the use of simple interpolations, to obtain quantitative predictions on the resulting material properties. Numerical results obtained with the proposed crease model show good agreement in comparison to experimental results published in the literature (Nagasawa et al., 2003), when the simulation of the standard bending test is performed. Application of the model to full-scale simulations is in progress and will be described in forthcoming publications.

Acknowledgments

The financial support by Tetra Pak Packaging Solutions is gratefully acknowledged. The second Author also acknowledges the support by MIUR-PRIN 2009AJ3PC9_004.

References

Beex, L.A.A., Peerlings, R.H.J., 2009. An experimental and computational study of laminated paperboard creasing and folding. International Journal of Solids and Structures 46 (24), 4192–4207.

Carlsson, L., De Ruvo, A., Fellers, C., 1983. Bending properties of creased zones of paperboard related to interlaminar defects. Journal of Materials Science 18 (5), 1365–1373.

Castro, J., Ostoja-Starzewski, M., 2003. Elasto-plasticity of paper. International Journal of Plasticity 19 (12), 2083–2098.

Cavlin, S., Dunder, I., Edholm, B., 1997. Creasability testing by inclined rules – a base for standardized specification of paperboard. Packaging Technology and Science 10 (4), 191–207.

Chai, H., Babcock, C., Knauss, W., 1981. One dimensional modelling of failure in laminated plates by delamination buckling. International Journal of Solids and Structures 17 (11), 1069–1083.

Giampieri, A., Perego, U., 2011. An interface finite element for the simulation of localized membrane-bending deformation in shells. Computer Methods in Applied Mechanics and Engineering 1. doi:10.1016/j.cma.2011.04.009.

Harrysson, A., Ristinmaa, M., 2008. Large strain elasto-plastic model of paper and corrugated board. International Journal of Solids and Structures 45 (11–12), 3334–3352.

Isaksson, P., Hagglund, R., 2005. A mechanical model of damage and delamination in corrugated board during folding. Engineering Fracture Mechanics 72 (15), 2299–2315.

Lemaitre, J., Chaboche, J.L., 1994. Mechanics of Solid Materials. Cambridge University Press.

Makela, P., Östlund, S., 2003. Orthotropic elastic–plastic material model for paper materials. International Journal of Solids and Structures 40 (21), 5599–5620.

Nagasawa, S., Fukuzawa, Y., Yamaguchi, T., Tsukatani, S., Katayama, I., 2003. Effect of crease depth and crease deviation on folding deformation characteristics of coated paperboard. Journal of Materials Processing Technology 140 (1–3), 157–162.

Nagasawa, S., Endo, R., Fukuzawa, Y., Uchino, S., Katayama, I., 2008. Creasing characteristic of aluminum foil coated paperboard. Journal of Materials Processing Technology 201 (1–3), 401–407.

Nygårds, M., Hallbäck, N., Just, M., Tryding, J., 2005. A finite element model for simulations of creasing and folding of paperboard. In: 2005 Abaqus User's Conference, pp. 373–387.

Nygårds, M., Just, M., Tryding, J., 2009. Experimental and numerical studies of creasing of paperboard. International Journal of Solids and Structures 46 (11–12), 2493–2505.

Oakley, D., Knight, N.F., 1995a. Adaptive dynamic relaxation algorithm for non-linear hyperelastic structures part i. formulation. Computer Methods in Applied Mechanics and Engineering 126 (1–2), 67–89.

Oakley, D., Knight, N.F., 1995b. Adaptive dynamic relaxation algorithm for non-linear hyperelastic structures part ii. single-processor implementation. Computer Methods in Applied Mechanics and Engineering 126 (1–2), 91–109.

Sawyer, J.P.G., Jones, R., Mckinlay, P.R., 1998. A unified constitutive theory for paper. Composite Structures 42 (1), 93–100.

Stenberg, N., Fellers, C., östlund, S., 2001. Plasticity in the thickness direction of paperboard under combined shear and normal loading. Journal of Engineering Materials and Technology 123 (2), 184–190.

Thakkar, B.K., Gooren, L.G.J., Peerlings, R.H.J., Geers, M.G.D., 2008. Experimental and numerical investigation of creasing in corrugated paperboard. Philosophical Magazine 88 (28), 3299–3310.

Xia, Q.S., 2002. Mechanics of inelastic deformation and delamination in paperboard. Ph.D. Thesis; Massachusetts Institute of Technology, Massachusetts, USA.

Xia, Q., Boyce, M.C., Parks, D.M., 2002. A constitutive model for the anisotropic elastic-plastic deformation of paper and paperboard. International Journal of Solids and Structures 39 (15), 4053–4071.